Conformal invariance and the Ising model on a spheroid

Youjin Deng[1] and Henk W. J. Blöte[1,2]
[1]*Faculty of Applied Sciences, Delft University of Technology, P.O. Box 5046, 2600 GA Delft, The Netherlands*
[2]*Lorentz Institute, Leiden University, P.O. Box 9506, 2300 RA Leiden, The Netherlands*
(Received 13 November 2002; published 14 March 2003)

We formulate conformal mappings between an infinite plane and a spheroid, and one between a semi-infinite plane and a half spheroid. Special cases of the spheroid include the surface of an infinitely long cylinder, of a sphere, and of a flat disc. These mappings are applied to the critical Ising model. For the case of the sphere and the flat disc, we derive analytical expressions for the second and the fourth moments of the magnetization density, and thus for the Binder cumulant. Next, we investigate Ising models on spheroids and half spheroids by means of a continuous cluster Monte Carlo method for simulations in curved geometries. Fixed and free boundary conditions are imposed for half spheroids. The Monte Carlo data are analyzed by finite-size scaling. Critical values of the Binder cumulants and other ratios on the sphere and on the flat disc agree precisely with the exact calculations mentioned above. At criticality, we also sample two- and one-point correlation functions on spheroids on half spheroids, respectively. The magnetic and temperature scaling dimensions, as determined from the Monte Carlo data and the theory of conformal invariance, are in good agreement with exact results.

DOI: 10.1103/PhysRevE.67.036107 PACS number(s): 05.50.+q, 64.60.Cn, 64.60.Fr, 75.10.Hk

I. INTRODUCTION

In two dimensions, the consequences of conformal invariance for critical systems have been studied extensively. These studies have produced a large amount of results for both bulk and surface critical phenomena [1–4]. One of the reasons is that the conformal group in two dimensions is an infinite-parameter group, so that the restrictions imposed by conformal invariance are strong. As a result, the forms of the bulk and surface correlation functions, and thus the critical exponents are limited by conformal invariance. Under Cardy's mapping between an infinite plane and the surface of a cylinder [5], the algebraic decay of correlations in the plane is transformed into an exponential decay along the cylinder. By utilizing the Schwarz-Christoffel formula, Burkhardt and Eisenriegler conformally mapped the infinite plane onto a rectangular geometry [2]. Furthermore, Cardy and Burkhardt investigated the semi-infinite plane and the parallel-plate geometry with uniform or mixed boundary conditions [4,6]. The universal properties of a system inside a circle with free or fixed boundary conditions have been studied both exactly and numerically [2,3,7].

However, as far as we know, no applications of conformal mappings onto curved geometries have been reported in two dimensions. In this paper, we use a conformal mapping of an infinite plane onto a spheroid. By rotating an ellipse about the minor or the major axis, one obtains an oblate or a prolate spheroid, respectively. Special cases include the surface of an infinitely long cylinder, of a sphere, and of a flat disc. The latter case is reached when the polar diameter of the spheroid approaches zero, so that one obtains the interiors of two circles connected at their perimeters. Thus, this transformation includes Cardy's mapping as a special case. We also perform a different conformal mapping from a semi-infinite plane onto a half spheroid.

We apply these mappings to the critical Ising model. From the known bulk two- and four-point correlation functions in the plane, and the assumption of covariance of the multipoint correlations under conformal mappings, the second and the fourth moments of the magnetization density σ on the sphere and on the flat disc can be expressed in terms of integrals. Since a direct analytic calculation of most of these integrals is not feasible, we evaluated them by means of Monte Carlo integration. As a result, we obtain the universal quantity $Q=\langle\sigma^2\rangle^2/\langle\sigma^4\rangle$, and ratios $r_2=\langle\sigma^2\rangle_s/\langle\sigma^2\rangle_d$ and $r_4=\langle\sigma^4\rangle_s/\langle\sigma^4\rangle_d$, where the subscripts s and d represent the sphere and the flat disc, respectively.

The nonzero net curvature of a spheroid poses a problem for numerical applications of conformal invariance. The difficulty is that a system defined on the spheroid seems to defy any acceptable discretization. Even if the net curvature of a given geometry is zero, numerical simulations may be complicated due to the presence of curved boundaries. An example is a system inside a circle. Badke *et al.* and Rěs and Straley have approximated this geometry for the Ising model. A circle is drawn on a square lattice and then free or fixed boundary conditions are imposed by removing or freezing the spins outside the circle, respectively [3,7]. The effectivity of this approximation is, however, somewhat limited because of irregular finite-size behavior, as shown later.

Recently, a continuous cluster Monte Carlo algorithm has become available for the anisotropic limit of the lattice Ising model [8,9]. One of the interesting properties of this model is that one of its dimensions is continuous, which enables one to apply the continuous cluster method to curved geometries such as a spheroid. Using a Wolff-like version of this algorithm [9], we investigate the Ising model on several spheroids, including a sphere, a flat disc, and a prolate spheroid. Near the critical point, we sampled the moments of the magnetization density and the quantity Q. The Monte Carlo data were analyzed by means of finite-size scaling. For the sphere and the flat disc, the numerical results for the ratios Q, r_2 and r_4 are in excellent agreement with the aforementioned exact calculations, which will be presented in detail in Sec. III. At criticality, the two-point magnetic correlations were sampled. Moreover, the Ising model on half spheroids was studied,

including that on a half sphere and inside a circle. Both fixed and free boundary conditions were used. The density profiles of the magnetization and of the energy, i.e., one-point correlations, were sampled. From the Monte Carlo data and the theory of conformal invariance, we determined the magnetic and temperature scaling dimensions with a satisfactory precision.

The outline of this paper is as follows. In Sec. II, we formulate the transformations of the infinite plane into the spheroid and the semi-infinite plane into the half spheroid. For systems on a spheroid and on a half spheroid, the forms of the two- and one-point correlation functions, respectively are derived. In Sec. III, we perform exact calculations of moments of the magnetization density on the sphere and on the flat disc. Section IV summarizes the Hamiltonian limit of the Ising model and the continuous cluster method for curved space. The numerical results are presented in Sec. V. Finally, we give a short discussion in Sec. VI.

II. CONFORMAL MAPPING

In three-dimensional Cartesian coordinates (x,y,z), a spheroid can be defined by

$$\frac{x^2}{a^2}+\frac{y^2}{a^2}+\frac{z^2}{b^2}=1 \quad (a,b>0), \tag{1}$$

where a and b are the equatorial and the polar radii, respectively. The parametric equations for the spheroid are therefore

$$x=a\sin\theta\sin\psi, \quad y=a\sin\theta\cos\psi, \quad z=b\cos\theta, \tag{2}$$

in which $0\leqslant\theta\leqslant\pi$ and $0<\psi\leqslant 2\pi$. Thus, the line element of the spheroid is

$$\begin{aligned} ds'^2 &= dx^2+dy^2+dz^2=(a^2\cos^2\theta+b^2\sin^2\theta)d\theta^2 \\ &\quad + a^2\sin^2\theta\, d\psi^2 = dw^2+f(w)\, d\psi^2. \end{aligned} \tag{3}$$

Here, we have defined a new coordinate w to specify the distance along the ellipse from the 'north pole' as a function of θ (see Fig. 1). The coordinate w is related to the parameter θ by $w=\int_0^\theta \sqrt{a^2\cos^2 v+b^2\sin^2 v}\, dv$, which is an elliptic integral of the second kind, and $f(w)=a^2\sin^2\theta$.

In polar coordinates (r,φ), the line element in an infinite plane is

$$ds^2=dr^2+r^2\, d\varphi^2. \tag{4}$$

A conformal transformation from the infinite plane into the spheroid is thus established by the equations

$$r=e^{-g(\theta)}, \quad \text{and} \quad \varphi=\psi,$$

$$\text{with } g(\theta)=\int^\theta \sqrt{(b/a)^2+\cot^2 v}\, dv, \tag{5}$$

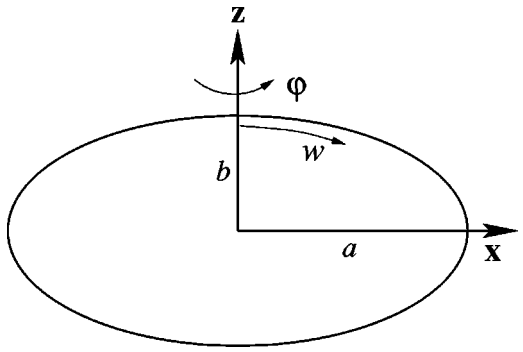

FIG. 1. Example of an ellipse with $1/e=a/b=2$. The corresponding oblate spheroid is obtained by the rotation of the ellipse about the z direction. The new coordinate w specifies the distance along the ellipse from the north pole.

and by the requirement that the points $r=0$ and $r=\infty$ are mapped onto points $\theta=\pi$ and 0, respectively. Transformation (5) is conformal, because the line elements Eqs. (4) and (3) differ only by a position-dependent factor:

$$ds^2=ds'^2[e^{-2g(\theta)}/a^2\sin^2\theta]. \tag{6}$$

Under a conformal mapping $(\vec{r}\to\vec{r}')$, a multipoint correlation function covariantly transforms as [1]

$$\begin{aligned} \langle\sigma_1(\vec{r}_1)\sigma_2(\vec{r}_2)\cdots\rangle_{\vec{r}} &= b(\vec{r}_1)^{-X_1}b(\vec{r}_2)^{-X_2}\cdots \\ &\quad\times\langle\sigma_1(\vec{r}_1')\sigma_2(\vec{r}_2')\cdots\rangle_{\vec{r}'}, \end{aligned} \tag{7}$$

where σ_i is a scaling operator (e.g., associated with the magnetization density or the energy density), X_i is the corresponding scaling dimension, and $b(\vec{r})$ is the rescaling factor, which reads $b(\vec{r})^2=ds^2/ds'^2$.

In the infinite plane, the bulk two-point correlation function at criticality behaves as [10]

$$\langle\sigma(\vec{r}_1)\sigma(\vec{r}_2)\rangle_{\text{plane}}=B|\vec{r}_2-\vec{r}_1|^{-2X}, \tag{8}$$

where B is a constant. Thus, according to Eqs. (5)–(8), one obtains the correlation function $g_1(\theta)$ of two points (θ,ψ) and $(\theta,\psi+\pi)$ on a spheroid $(\psi\leqslant\pi)$

$$g_1(\theta)=B(2a\sin\theta)^{-2X}. \tag{9}$$

The evaluation of the mapping formula [Eq. (5)] is complicated in general. However, for the special cases mentioned above, it simplifies and yields more results.

(i) *Surface of a cylinder*. As the polar radius $b\to\infty$, the spheroid approaches the surface of an infinitely long cylinder. The substitutions of a new coordinate $u=b\theta$ and the radius $R=a$ of the cylinder lead to

$$ds'^2=du^2+R^2 d\psi^2 \quad (-\infty<u<\infty, 0<\psi\leqslant 2\pi), \tag{10}$$

and the mapping formula [Eq. (5)] simplifies to

$$r = e^{-u/R} \quad \text{and} \quad \varphi = \psi. \tag{11}$$

Thus, Cardy's mapping is restored [5]. The critical two-point correlation functions along the cylinder are then

$$\langle \sigma(u_1,\psi)\sigma(u_2,\psi)\rangle = BR^{-2X}e^{-X|u_1-u_2|/R} \times (1-e^{-|u_1-u_2|/R})^{-2X}. \tag{12}$$

So the correlations decay exponentially for $|u_1-u_2| \gg 0$.

(ii) *Surface of a sphere*. One obtains a sphere when the polar and the equatorial radii are equal, i.e., $b=a=R$. The line element Eq. (3) reduces to $ds'^2 = R^2\,(d\theta^2 + \sin^2\theta d\psi^2)$, and the mapping formula becomes

$$r = 2R\cot(\theta/2) \quad \text{and} \quad \varphi = \psi. \tag{13}$$

A geometric picture of this mapping involves the placement of a sphere with radius R on top of an infinite plane (Fig. 2). The mapping of a point $\vec{r}$ in the plane on the sphere is defined as the intersection between the sphere and the line connecting the north pole and the point $\vec{r}$. Here, the vector $\vec{r}$ stands for the point (r,φ) in Eq. (13). According to Eqs. (7), (8), and (13), one has the pair correlation function on the sphere as

$$\langle \sigma(\theta_1,\psi_1)\sigma(\theta_2,\psi_2)\rangle = BR^{-2X}2^{-X}[1-\sin\theta_1\sin\theta_2 \times\cos(\psi_1-\psi_2)-\cos\theta_1\cos\theta_2]^{-X}. \tag{14}$$

If one introduces $\vec{R}$ to represent the vector from the center of the sphere to the point (θ,ψ), Eq. (14) reduces to

$$\langle \sigma(\vec{R}_1)\sigma(\vec{R}_2)\rangle = B|\vec{R}_1-\vec{R}_2|^{-2X}, \tag{15}$$

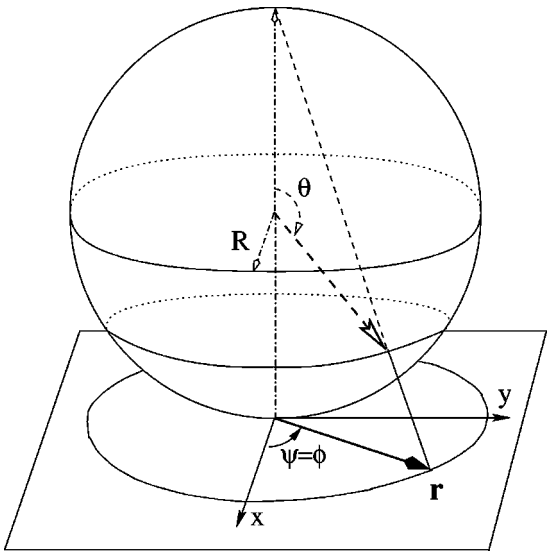

FIG. 2. Illustration of the conformal mapping of an infinite plane on the surface of a sphere.

which, interestingly, has the same form as Eq. (8).

(iii) *Surface of a flat disc*. In the limit $b \to 0$ of an oblate spheroid, a flat-disc geometry is reached. The coordinate w and the element (3), respectively, reduce to

$$w = a\sin\theta \quad \text{and} \quad ds'^2 = dw^2 + w^2 d\psi^2 \quad (w \leqslant R = a), \tag{16}$$

and the mapping formula becomes

$$r = \begin{cases} w/R & 0 \leqslant r < 1 \\ R/w & r \geqslant 1. \end{cases} \tag{17}$$

This mapping can be generalized to any number of dimensions.

Under the mapping Eq. (17), one finds two formulas for $g(\vec{w}_1,\vec{w}_2) = \langle \sigma(\vec{w}_1)\sigma(\vec{w}_2)\rangle$, of which the applicability depends on whether or not the two points $\vec{r}_1$ and $\vec{r}_2$ lie in the same face of the flat disc:

$$g(\vec{w}_1,\vec{w}_2) = \begin{cases} B[w_1^2+w_2^2-2w_1w_2\cos(\psi_1-\psi_2)]^{-X} & (\vec{w}_1,\vec{w}_2\text{: same face}) \\ B[(w_1w_2)^2+R^2-2w_1w_2\cos(\psi_1-\psi_2)]^{-X} & (\vec{w}_1,\vec{w}_2\text{: opposite faces}), \end{cases} \tag{18}$$

where we have introduced $\vec{w}$ to represent the vector from the center of the disc to the point (w,ψ).

The derivative $\partial r/\partial w$ in the Eq. (17) is discontinuous at the edge $w=R$. One may thus expect that finite-size corrections arise for the critical behavior near the edge.

Next, we describe the conformal transformation between a semi-infinite plane and a half spheroid. The latter object is defined by Eq. (1) but with $z \leqslant 0$. The mapping can conveniently be described in two steps. First, one parametrizes the plane complex numbers $z=x+iy$, so the formula $z'=(z-i)/(z+i)$ maps the semi-infinite plane $\mathbb{R}\times\mathbb{R}^+$ onto the interior of a unit circle (Fig. 3) [1]. This conformal mapping yields the profile of a scaling operator inside a unit circle as

$$\langle \sigma(r')\rangle = (1-r'^2)^{-2X}. \tag{19}$$

This result can be generalized to any number of dimensions [1,2]. Second, the interior of the unit circle is conformally

mapped on the half spheroid under the transformation Eq. (5). In the limit $b\to\infty$, a semi-infinite cylinder [Eq. (10) but with $u\geqslant 0$] is reached, on which the profile of a scaling operator behaves as

$$\langle\sigma(u)\rangle\propto R^{-X}e^{-uX/R}(1-e^{uX/2R})^{-X}. \tag{20}$$

For $b=a=R$ a half spheroid reduces to a half sphere, and one has

$$\langle\sigma(\theta)\rangle\propto(R\cos\theta)^{-X}. \tag{21}$$

III. EXACT CALCULATION

Since the transformations between the plane and the special cases of the spheroid [Eqs. (11), (13), and (17)] are relatively simple, it is possible to derive the expressions for $\langle\sigma^2\rangle$ and $\langle\sigma^4\rangle$ from the exact solution of the Ising model in the infinite plane [10]. For the case of an infinitely long cylinder, Burkhardt has evaluated these expressions by means of Monte Carlo integration [11]. The result is consistent with that obtained from direct simulations of systems on the cylinder [11]. Here, we follow analogous procedures for the surface of a sphere and of a flat disc.

In the continuum limit, the second and fourth moments of the magnetization density $\langle\sigma^2\rangle$ and $\langle\sigma^4\rangle$ can be given in terms of the two- and four-spin correlation functions, respectively:

$$\langle\sigma^2\rangle=\rho^2\int \mathrm{d}S_1\mathrm{d}S_2 g(\vec{r}_1,\vec{r}_2), \quad \text{and}$$

$$\langle\sigma^4\rangle=\rho^4\int \mathrm{d}S_1\cdots\mathrm{d}S_4 g(\vec{r}_1,\vec{r}_2,\vec{r}_3,\vec{r}_4), \tag{22}$$

where ρ is the areal density of the spins, and $\mathrm{d}S_i$ represents the number of spins in an infinitesimal area. For a sphere, ρ and $\mathrm{d}S_i$ can be written as $1/(4\pi R^2)$ and $R^2\sin\theta_i\mathrm{d}\theta_i\mathrm{d}\psi_i$, respectively. For a flat disc, $\rho=1/(2\pi R^2)$ and $\mathrm{d}S_i=r_i\mathrm{d}r_i\mathrm{d}\psi_i$. R is the radius of the sphere or the flat disc. $g(\vec{r}_1,\vec{r}_2)$ and $g(\vec{r}_1,\vec{r}_2,\vec{r}_3,\vec{r}_4)$ are the two- and four-spin correlation functions.

The two-point correlation function is known exactly [Eq. (8)]. An exact result is also available for the bulk four-spin correlation of the two-dimensional critical Ising model, which is given in terms of pair correlations by [12]

$$g(1,2,3,4)=\frac{1}{2}\left\{\left[\frac{g(1,2)g(2,3)g(3,4)g(4,1)}{g(1,3)g(2,4)}\right]^2+(2\leftrightarrow 3)+(3\leftrightarrow 4)\right\}^{1/2}. \tag{23}$$

Here, for simplicity, we have written $g(\vec{r}_1,\vec{r}_2)$ and $g(\vec{r}_1,\vec{r}_2,\vec{r}_3,\vec{r}_4)$ as $g(1,2)$ and $g(1,2,3,4)$, respectively. The notation $(i\leftrightarrow j)$ represents the expression between square brackets [ ] with i and j interchanged.

The universal amplitude ratio $Q=\langle\sigma^2\rangle^2/\langle\sigma^4\rangle$ is simply related to the Binder cumulant [13].

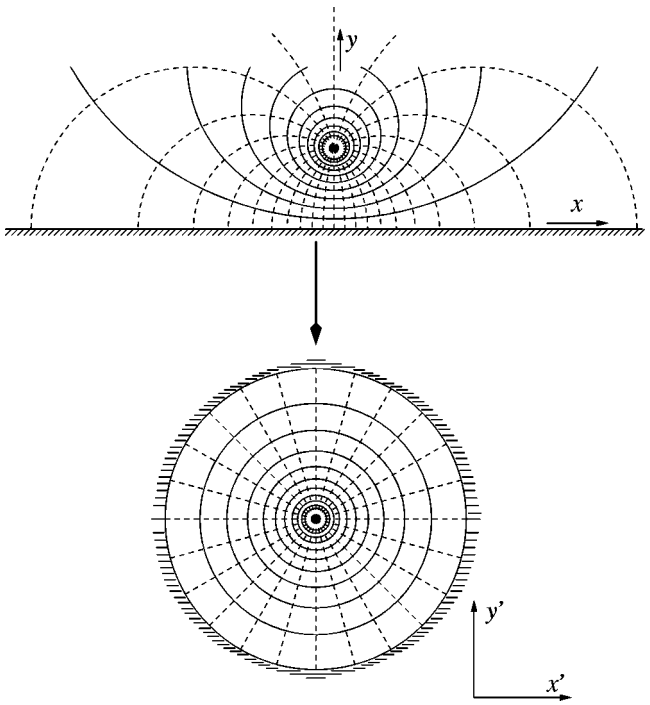

FIG. 3. Illustration of the conformal mapping from a semi-infinite plane on a single disc.

(i) *Surface of a sphere*. The substitution of the pair correlation on a sphere [Eq. (14)] leads to

$$\begin{aligned}\langle\sigma^2\rangle&=\rho^2 4\pi R^2\int_0^{2\pi}\mathrm{d}\psi_2\int_0^{\pi}\mathrm{d}\theta_2 R^2\sin\theta_2 g(0,0;\theta_2,\psi_2)\\&=BR^{-2X}2^{-X-1}\int_0^{\pi}\mathrm{d}\theta_2\sin\theta_2(1-\cos\theta_2)^{-X}\\&=BR^{-2X}2^{-2X}/(1-X),\end{aligned} \tag{24}$$

for the Ising model, $X=2-y_h=1/8$ so that $\langle\sigma^2\rangle=(2^{11/4}/7)BR^{-2X}\approx 0.961\,024\,5BR^{-2X}$.

Equations (22) and (23) and substitutions of the integration variables $x_i=\theta_i/\pi$ and $y_i=\psi_i/2\pi$ lead to

$$\langle\sigma^4\rangle=BR^{-4X}\pi^3 2^{-2X-3}\times\int_0^1\mathrm{d}x_2\mathrm{d}x_3\mathrm{d}x_4\mathrm{d}y_3\mathrm{d}y_4 f(x_2;x_3,y_3;x_4,y_4) \tag{25}$$

with $f(x_2;x_3,y_3;x_4,y_4)=\sin(\pi x_2)\sin(\pi x_3)\sin(\pi x_4)\times g(1,2,3,4)$, where the coordinates of these four points are $(0,0)$, $(\pi x_2,0)$, $(\pi x_3,2\pi y_3)$, and $(\pi x_4,2\pi y_4)$. This equation was evaluated with a Monte Carlo procedure, which approximates the integral by

$$\langle \sigma^4 \rangle = BR^{-4X} \pi^3 2^{-2X-3} N^{-1} \sum_{i=1}^{N} f(x_2^{(i)}; x_3^{(i)}, y_3^{(i)}; x_4^{(i)}, y_4^{(i)}), \tag{26}$$

where $x^{(i)}$ and $y^{(i)}$ are uniformly distributed random numbers in the interval (0,1). It yields $\langle \sigma^4 \rangle = BR^{-4X}(1.198\,78 \pm 0.000\,02)$, where the two decimal numbers are the average and standard error obtained from 1000 determinations of the integral. Each integral involves 10^6 Monte Carlo steps.

Thus, the value of the dimensionless quantity is obtained as $Q = 0.770\,42 \pm 0.000\,01$.

(ii) *Surface of a flat disc.* The critical pair correlations on a flat disc are given by Eq. (18). The evaluations both of $\langle \sigma^2 \rangle$ and $\langle \sigma^4 \rangle$ were done by means of Monte Carlo procedures because in this case the symmetry lower than that of a sphere. The calculation must allow for the fact that the form of the pair correlation depends on whether or not the two points are in the same face [Eq. (18)]. Taking into account all possible distributions of the four correlated points, one finds

$$\langle \sigma^4 \rangle = \rho^4 \int_0^R dr_1 \cdots dr_4 \int_0^{2\pi} d\psi_1 \cdots d\psi_4 \times r_1 r_2 r_3 r_4 [2g_0(1,2,3,4) + 8g_1 + 6g_2], \tag{27}$$

where $g_0(1,2,3,4)$ defines correlations of four points on the same face, g_1 applies to three points on one face and one on the other, and g_2 applies to two points on one face and two on the other. From this calculation, we obtain $\langle \sigma^2 \rangle = R^{-2X}(1.041\,56 \pm 0.000\,01)$, $\langle \sigma^4 \rangle = R^{-4X}(1.412\,73 \pm 0.000\,05)$, and thus $Q = 0.767\,91 \pm 0.000\,03$.

The ratios of moments of the magnetization density on the sphere and on the flat disc are thus given as

$$r_2 = \langle \sigma^2 \rangle_s / \langle \sigma^2 \rangle_d = 0.922\,68(2)$$

$$\text{and } r_4 = \langle \sigma^4 \rangle_s / \langle \sigma^4 \rangle_d = 0.848\,57(4), \tag{28}$$

where the number between parentheses stands for the estimated error in the last decimal place.

IV. MODEL AND ALGORITHM

As mentioned before, simulations on a spheroid are difficult due to the incompatibility of regular lattices with curved geometries. Here, we tackle this problem by using the Hamiltonian limit of a two-dimensional lattice Ising model. For such a system, an efficient continuous Wolff-like method has been explained in detail [9]. Here, we describe the application of this algorithm to simulations in curved geometries.

The Hamiltonian of an Ising model on a $L \times L$ square lattice with periodic boundary conditions reads

$$\mathcal{H}/k_B T = -\sum_{x,y} [K_x \sigma_{x,y} \sigma_{x+1,y} + K_y \sigma_{x,y} \sigma_{x,y+1}], \tag{29}$$

where the integers $1 \leqslant x, y \leqslant L$ label the lattice sites. K_x and K_y are the coupling strengths along the x and y direction, respectively. The spins can assume the values $\sigma_{x,y} = \pm 1$. The critical line of this model is given by [10]

$$\sinh(2K_x)\sinh(2K_y) = 1. \tag{30}$$

In the anisotropic limit $\epsilon \to 0$, the couplings therefore are

$$K_x = \epsilon/t, \quad \exp(-2K_y) = \epsilon, \tag{31}$$

where t is a temperaturelike parameter whose critical point is $t_c = 1$. It is known that in this limit the system is equivalent to the quantum transverse Ising chain [14,15] with nearest-neighbor couplings and an external field t:

$$\mathcal{H}_{QM} = -\sum_x (\sigma_x^z \sigma_{x+1}^z + t\sigma_x^x), \tag{32}$$

with σ^z and σ^x Pauli matrices.

Since our purpose is the application of conformal invariance, we have to restore isotropy asymptotically for the system with $K_x < K_y$. This can be done by increasing the number of spins in the y direction by a factor $L_y/L_x = \sinh 2K_y = 1/2\epsilon$ [16]. Meanwhile, one rescales the y direction as $y' = 2y/\epsilon$ so that the system sizes along the x and y direction are equal again, $L_y' = L_x$. As a result, the y dimension becomes continuous as $\epsilon \to 0$, i.e., there is an infinite number of spins per physical length unit, and the lattice structure transforms into L lines of length L. The spins form ranges of $+/-$ signs, and the number of interfaces in the system is of order L^2.

For this anisotropic limit, a full description of the aforementioned continuous Wolff-like algorithm has been given in Ref. [9]. For the convenience of the reader, we summarize the essential points. During the formation of a cluster, a bond between nearest-neighboring spins with the same sign is "frozen" with a probability $P = 1 - \exp(-2K)$ or "broken" with $1 - P$. Sites connected by frozen bonds are included in the same cluster. For the anisotropic limit, the probability P in the x and y direction will be of order ϵ and $1 - \epsilon$, respectively. Thus, the strong-couping bonds will continue to connect spins in the y direction until a break occurs with a probability of order ϵ per bond. Therefore, after the rescaling discussed above, the connected spins along the lines in the y direction form ranges of $+/-$ signs with lengths of order 1, and the breaks are just the aforementioned interfaces. Moreover, the average distance of the bonds between adjacent lines is also of order 1. These weak-coupling bonds serve as "bridges" between neighboring lines to connect ranges of the same sign, and help to build clusters. Analogous to cluster methods for the discrete models, the aforementioned continuous cluster algorithm flips one or more clusters during a Monte Carlo step depending on whether it is Wolff-like or Swendsen-Wang-like. The correctness and efficiency of this method has been demonstrated both in two and three dimensions [9].

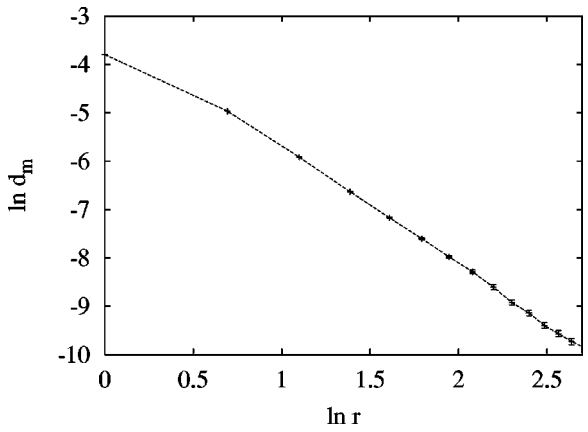

FIG. 4. Decay of the difference $d_m(r)$ of the magnetic correlation functions in the x and y direction, shown as $\ln d_m$ vs $\ln r$. The system size is 40×40.

Although the long-distance behavior of such an anisotropic system is the same in the x and y direction, corrections may exist at short distances. We investigate this problem in a system with size $L=40$. We sampled the difference $d_m(r)$ of the magnetic correlation functions over distances r in the x and y direction

$$d_m(r)=\frac{1}{V}\sum_x \int \mathrm{d}y\langle \sigma_{x,y}\sigma_{x+r,y}-\sigma_{x,y}\sigma_{x,y+r}\rangle, \quad (33)$$

where $V=\Sigma_x\int \mathrm{d}y=L\times L$ is the area of the square. A plot of d_m as a function of r is shown in Fig. 4. The fact that the line becomes approximately straight at the right-hand side indicates that the leading correction behaves as r^{y_a}. From Fig. 4, we estimate the associated exponent $y_a\approx -2.25$, so we simply assume that $y_a=-2X_h+y_i$, where $y_i=-2$ is the correction-to-scaling exponent in the two-dimensional Ising model, and $X_h=1/8$ is the magnetic scaling dimension. Taking into account the periodic boundary conditions, we fitted the Monte Carlo data according to the least-squares criterion on the basis of

$$d_m=r^{-2X_h}\{a_1\,[r^{y_i}+(L-r)^{y_i}]+a_2[r^{y_1}+(L-r)^{y_1}]\}, \quad (34)$$

where a_1, a_2 are unknown parameters, and the term with $y_1=-3$ is another significant correction. We obtain $a_1=0.022\,8(6)$ and $a_2=0.027(3)$.

Since the model is now continuous in the y direction, one can investigate it in curved geometries such as a spheroid. As an example, we consider the case of a sphere S^2. The structure of the anisotropic model in the flat geometry defined by Eqs. (29) and (31) consists of L lines of length L. Each of these lines can be understood as a circle S^1 because of the periodic boundary condition. As a result, one can represent the ''lattice structure'' on a sphere S^2 by L uniformly distributed circles with varying radius (Fig. 5), such that there are strong couplings along the circles while weak couplings occur between adjacent circles. The location of the kth circle is

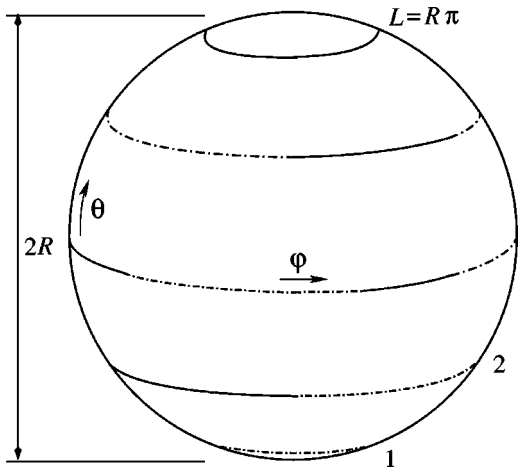

FIG. 5. Example of ''lattice structure'' on a sphere, on which $L=5$ circles represent continuous lines of spins in the strong-coupling direction. The full and dash-dotted parts of the circles represent (arbitrarily chosen) ranges of spins with different signs.

$\theta_k=(k-\frac{1}{2})\pi/L$, with $k=1,2,\ldots,L$ (Fig. 5), and the corresponding circumference is $c_k=2L\sin\theta_k$, which accounts for the S^2 curvature. Since the probability of a weak-couping bond is defined *per unit of length*, and the adjacent circles on a sphere have different radii, the distribution of these weak-coupling bonds still requires a length scale. It was chosen as the average length scale of both circles. Self-interactions via weak bonds over the poles $\theta=0$ or π could, in principle, occur at the circles with $k=1$ and L, respectively. But these interactions may be set to zero because the circles at $\theta=0$ and π have a zero length. By means of the continuous Wolff-like algorithm, we simulated the above model on a sphere. The magnetic correlation of diametrically opposite points was sampled,

$$g_0(\theta)=\frac{1}{\pi}\int_0^{\pi}\mathrm{d}\psi\langle\sigma(\theta,\psi)\sigma(\pi-\theta,\psi+\pi)\rangle. \quad (35)$$

An example for systems without self-interactions at $\theta=0$ and π is shown in Fig. 6. As the number of the circles L increases, the pole $\theta=0$ is approached, and the spacing of adjacent circles decreases. The lines are quite straight, which indicates that the spherical symmetry is restored asymptotically. We have also investigated the system with self-interactions over the poles. Significant deviations from isotropy occur in this case.

On a microscopic scale, the lattice structure on a sphere is the same as that on a flat plane. However, for finite L, apart from microscopic deviations from the uniformity, the discretization in θ may lead to a global effect on the coupling strength. According to the trapezium rule, we expect that this deviation vanishes as L^{-2}. Under renormalization this effect leads to corrections proportional to L^{y_t-2}, where $y_t=1$ is the temperature renormalization exponent. Thus, this effect vanishes when $L\to\infty$, and the critical point on a sphere is identical to that on the flat plane. Moreover, since the exponent of

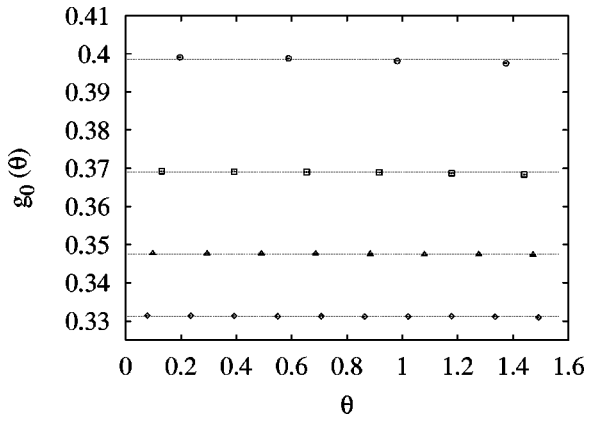

FIG. 6. The magnetic correlation functions $g_0(\theta)$ on spheres vs θ. The Monte Carlo data are shown for system sizes $L=8$ (○), $L=12$ (□), $L=16$ (△), and $L=20$ (◇). The lines show the corresponding fits. The angle θ is given in radians.

the irrelevant field $y_i=-2$, it is expected that the term with L^{y_t-2} dominates over the corrections of order L^{y_i}, as will be confirmed later.

As an alternative way for the distribution of L circles on a sphere, the location of the kth circle can be given by $\theta_k=(k-1)\pi/(L-1)$, so that in this case the circumference of the sphere is $c=2(L-1)$. It was found numerically that the spherical symmetry is less well restored in this case. That may be due to the singularity of the zero radii of the circles with $k=1$ and L.

The same procedure can be applied to the disc geometry. The kth circle is simply located at $r_k=(k-1)$ and its circumference is given by $c_k=2\pi(k-1)$, with $k=1,2,\ldots,L$. For a general spheroid with constant ratio $e=b/a$, the problem that the circles should be evenly distributed is solved in two steps. First, since the circumference of the corresponding ellipse is $2L$, the value of the parameter a can be numerically calculated from the equation $L=a\int_0^L \mathrm{d}w = a\int_0^\pi \mathrm{d}\theta\sqrt{\cos^2\theta+e^2\sin^2\theta}$. Second, the location of the kth circle can be obtained by solving for θ_k in the equation $k-\frac{1}{2}=a\int_0^{\theta_k}\mathrm{d}\theta\sqrt{\cos^2\theta+e^2\sin^2\theta}$. The corresponding circumference is $c_k=2\pi a\sin\theta_k$ $(k=1,2,\ldots,L)$.

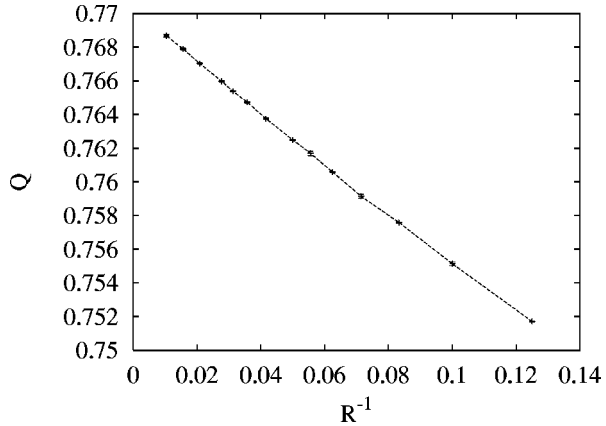

FIG. 7. The dimensionless quantity Q_R at criticality vs R^{-1}.

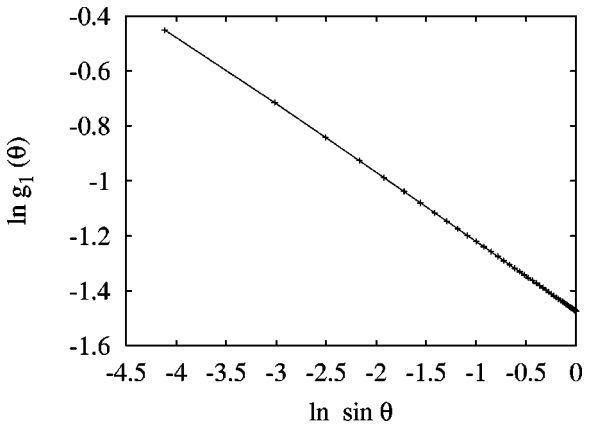

FIG. 8. Decay of the magnetic correlation function $g_1(\theta)$, shown as $\ln g_1(\theta)$ vs $\ln\sin\theta$. The number of circles on the sphere is $L=96$. The line shows the corresponding fit.

V. NUMERICAL RESULTS

By means of the continuous Wolff-like algorithm, we performed simulations of the Ising model on a sphere, on a flat disc, on a spheroid with $e=2$, on a half sphere, and inside a circle.

(i) *Surface of a sphere*. For systems on a sphere, we sampled $\langle\sigma^2\rangle$, $\langle\sigma^4\rangle$, and $Q_R(t)$ near the critical point. In addition, the two-point magnetic correlation function $g_1(\theta)=\langle\sigma(\theta,\psi)\sigma(\pi-\theta,\psi)\rangle$ was determined at criticality. The system sizes are taken as 15 values ranging from $L=8$ to 96. According to finite-size scaling, in the critical region, $Q_R(t)$ behaves as

$$Q_R(t)=Q_c+a_1R^{y_t}(t-t_c)+a_2R^{2y_t}(t-t_c)^2+\cdots+b_1R^{y_c}+b_2R^{y_i}+\cdots, \tag{36}$$

where a_1,a_2,b_1, and b_2 are unknown parameters, and Q_c is the universal value for the infinite system at criticality. The correction with exponent $y_c=y_t-2=-1$ is due to the discretization of the sphere as explained above. An example is shown in Fig. 7. The approximate linearity indicates that the approach of $Q_R(0)$ to Q_c occurs as R^{-1}. Formula (36) was fitted to Monte Carlo data according to the least-squares criterion. The value of the temperature parameter is fixed at $t_c=1$. We obtain $Q_c=0.770\,43(3)$, which is consistent with the exactly calculated value $0.770\,42(1)$ in Sec. III.

Similarly, the finite-size behavior of $\langle\sigma^2\rangle$ is

$$\langle\sigma^2\rangle=R^{-2X_h}[m_2+a_1R^{y_t}(t-t_c)+a_2R^{2y_t}(t-t_c)^2+\cdots+b_1R^{y_c}+b_2R^{y_i}+\cdots] \tag{37}$$

and that of $\langle\sigma^4\rangle$ is

$$\langle\sigma^4\rangle=R^{-4X_h}[m_4+a_1R^{y_t}(t-t_c)+a_2R^{2y_t}(t-t_c)^2+\cdots+b_1R^{y_c}+b_2R^{y_i}+\cdots]. \tag{38}$$

TABLE I. Fits of the correlation functions $g_1(\theta)$ on spheres.

$L_{\min}$	$L_{\max}$	$\theta_{\max}$	X_h	a_0	a_1	a_2
8	96	1.40	0.12497(4)	0.72215(5)	−0.026(2)	−0.023(4)
a_3	b_0	b_1	c			
−0.0006(1)	−0.427(3)	0.21(2)	−0.209(3)			

The exponents $-2X_h$ and $-4X_h$ of R are obtained by the substitution of $X_h=1/8$. The fits yield $m_2=0.619\,88(3)$ and $m_4=0.498\,75(5)$.

According to Eq. (14), $g_1(\theta)\propto(L\cos\theta)^{-2X_h}$, which is confirmed numerically in Fig. 8. On the basis of finite-size scaling and conformal invariance, the correlation function $g_1(\theta,L)$ is expected to behave as

$$g_1(\theta,L)=L^{-2X_h}\{(\cos\theta)^{-2X_h+cL^{y_c}}[a_0+a_1(L\pi-L\theta)^{y_c}+a_2(L\pi-L\theta)^{y_i}+a_3(L\sin\theta)^{y_c}]+b_0L^{y_c}+b_1L^{y_i}\}, \tag{39}$$

where a_0,a_1,a_3,b_0,b_1,c are unknown parameters. The corrections with amplitudes a_1 and a_2 are due to the deviations from isotropy at short distances; the term with a_3 accounts for the inhomogeneity because of the discretization of the θ direction. Equation (39) was fitted to the Monte Carlo data. As a consistency test, we choose X_h as a free parameter. We obtain $X_h=0.124\,97(4)$, which is in a good agreement with the exact result $X_h=1/8$ (see Table I). Although the parameter a_3 is quite small, it is necessary to obtain a reasonable residual.

(ii) *Surface of a flat disc*. The system sizes on the flat-disc geometry were taken as values of 12 odd numbers ranging from $L=13$ to 91. The corresponding radii are $L/2$. Near the critical point, we sampled Q_R, $\langle\sigma^2\rangle$, and $\langle\sigma^4\rangle$. The finite-size behavior of these quantities also follows from Eqs. (36), (37), and (38), respectively. The fits yield that $m_2=0.671\,9(1)$, $m_4=0.587\,9(1)$, and $Q_c=0.768\,02(15)$, which agrees well with the exact calculation $Q_c=0.767\,91(3)$. Thus, we also obtain the ratios $r_2=0.922\,63(13)$ and $r_4=0.848\,41(14)$, which are consistent with Eq. (28).

At criticality, three types of two-point magnetic correlation functions were sampled. We denote $g_1(r)$ as the one between two points with same coordinates (r,ψ) but on opposite faces, and $g_2(r)$ and $g_3(r)$ as those between two points (r,ψ) and $(r,\psi+\pi)$ on opposite and on the same faces, respectively. On the basis of Eq. (18), one expects that

$$g_1(r)\propto(L-4r^2/L)^{-2X_h},\quad g_2(r)\propto(L+4r^2/L)^{-2X_h},\quad g_3(r)\propto r^{-2X_h}. \tag{40}$$

A plot for $g_2(r)$ is shown in Fig. 9. The curvature near $r=L/2$ is due to the discrete property of the derivative $\partial\vec{r}/\partial w$ in the mapping formula Eq. (17). We assume that this effect decays as in order of $(L/2-r)^{y_c}$ when r approaches zero. Thus, one can obtain the finite-size behavior of these quantities by including corrections in Eq. (40). For instance, the quantity $g_3(r)$ follows

$$g_3(r)=r^{-2X_h+cL^{y_c}}[a_0+a_1r^{y_c}+a_2r^{y_i}+d_1(L/2-r)^{y_c}+b_0L^{y_c}+\cdots]. \tag{41}$$

By introducing a cutoff at large r, we made fits for $g_1(r)$, $g_2(r)$, and $g_3(r)$ independently, and obtain $X_h=0.124\,92(9)$, $X_h=0.125\,01(16)$, and $X_h=0.125\,05(7)$, respectively, in good agreement with the exact result.

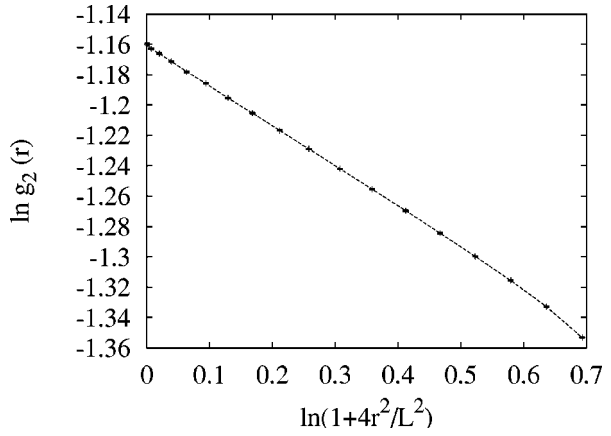

FIG. 9. Decay of the magnetic correlation function $g_2(r)$, shown as $\ln g_2(r)$ vs $\ln(1+4r^2/L^2)$. The finite-size parameter of the flat disc is $L=17$.

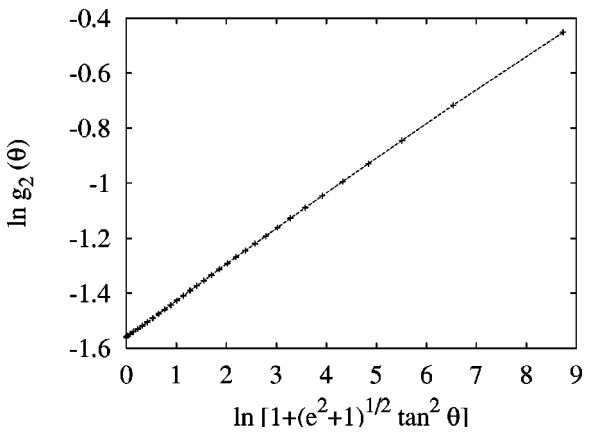

FIG. 10. Decay of the magnetic correlation function $g_2(\theta)$, shown as $\ln g_2(\theta)$ vs $\ln(1+\sqrt{e^2+1}\tan^2\theta)$. The finite size of the spheroid is $L=64$ and $e=b/a=2$.

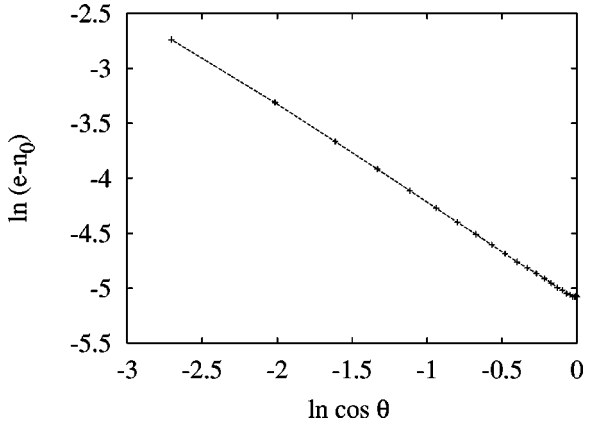

FIG. 11. Decay of the fluctuation of the energy density $e(\theta)-n_0$ for half the surface of a sphere, shown as $\ln(e-n_0)$ vs $\ln\cos\theta$. The system size $L=24$. n_0 is obtained from the Monte Carlo data for flat systems.

(iii) *Spheroids with* $e=2$. As an example, we performed Monte Carlo simulations for a prolate spheroid with the ratio $e=b/a=2$. We sampled the universal ratio Q_R and the magnetic correlation function $g_1(\theta)=\langle\sigma(\theta,\psi)\sigma(\theta,\psi+\pi)\rangle$. The analysis of the finite-size behavior of Q_R leads to the result $Q_c=0.764\,3(1)$. From the Monte Carlo data for $g_1(\theta)$ and Eq. (9), we obtain $X_h=0.124\,9(2)$.

We also sampled the correlation functions $g_2(\theta)=\langle\sigma(\theta,\psi)\sigma(\pi-\theta,\psi)\rangle$. The mapping formula is relatively complicated in this case, and we did not work out the expression of $g_2(\theta)$. But we observe that a plot of the Monte Carlo data $\ln[g_2(\theta)]$ versus $\ln(1+\sqrt{e^2+1}\tan^2\theta)$ approximately follows a straight line (Fig. 10). By means of finite-size scaling, we obtain the value of the slope as $0.124\,1(8)$, which is close to the exact result $X_h=1/8$.

(iv) *Half surface of a sphere with fixed boundary conditions*. We also investigated the anisotropic limit of the Ising model on a half sphere. An infinite ordering field was applied at the equator. The system sizes are taken as 10 values ranging from $L=4$ to 40. The corresponding radius is $R=(2L-1)/\pi$. We sampled the magnetization density $m=\langle\sigma(\theta)\rangle$

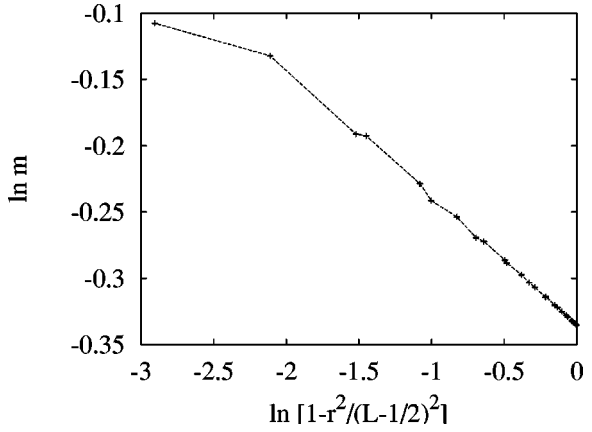

FIG. 12. Decay of the magnetization density $m=\langle\sigma(r)\rangle$, shown as $\ln m$ vs $\ln[1-r^2/(L-1/2)^2]$. The circle was cut from a $L\times L$ square lattice with $L=24$.

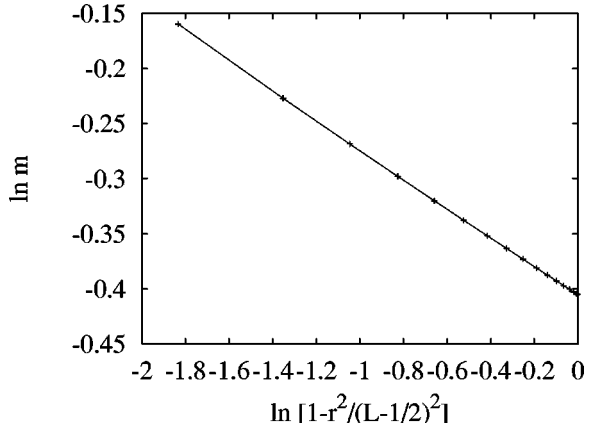

FIG. 13. Decay of the magnetization density $m=\langle\sigma(r)\rangle$, shown as $\ln m$ vs $\ln[1-r^2/(L-1/2)^2]$. The system size is $L=16$. Fixed boundary conditions were applied.

and the energy density e as a function of θ. Since the interactions along the θ and ψ direction are of different forms, the energy density can be represented in two ways: the interactions due to the weak-couplings $\langle\sigma(\theta)\sigma(\theta+1)\rangle$, or the density of interfaces along the strong-couplings $\langle n(\theta)\rangle$. We chose the latter because it needs much less computer time. The behavior of the magnetization density follows Eq. (20), and the energy density behaves as

$$e(\theta)=\langle n(\theta)\rangle=n_0+a(L\cos\theta)^{-X_t}, \tag{42}$$

where n_0 is the bulk density, and X_t is the temperature scaling dimension. An example is shown in Fig. 11. Finite-size analyses of the quantities $\langle\sigma(\theta)\rangle$ and $\langle e(\theta)\rangle$ yield $X_h=0.124\,99(2)$ and $X_t=0.995(6)$, respectively, which are again in excellent agreement with the exact values.

(v) *Interior of a circle*. Conformal invariance on the interior of a circle with free and fixed boundary conditions has been numerically tested by Badke *et al.*, and Rěs and Straley [3,7]. They approximated this geometry by drawing the circle from a square lattice. In this way, the symmetry along the ψ direction is broken, and irregular finite-size effects arise (Fig. 12). Thus, it seems appropriate to simulate the interior of a circle by means of the continuous algorithm. We used both free and fixed boundary conditions. The system sizes are taken as 10 values ranging from $L=8$ to 40. An example is shown in Fig. 13, and no irregular effects are observed. Analyses yield that $X_h=0.124\,994(15)$ and $X_t=1.002(7)$.

VI. DISCUSSION

Conformal invariance is known as a powerful tool to investigate critical behavior. Its applications in two dimensions have so far been focused on flat systems. We have shown how one can apply it in curved geometries. The validity of our method is confirmed by the agreement between predictions based on conformal invariance and our numerical results. Moreover, in the case of the Ising model, the difficulty of numerical simulations in curved geometries is solved by the recently developed continuous cluster algorithm. Trivial

modifications can generalize this algorithm to Potts models, including the percolation model [18].

Furthermore, since conformal mappings of three-dimensional systems usually lead to curved geometries, this algorithm enables us to investigate applications of conformal invariance in three dimensions [9,17,18].

ACKNOWLEDGMENTS

This research was supported by the Dutch FOM foundation (''Stichting voor Fundamenteel Onderzoek der Materie'') which is financially supported by the NWO (''Nederlandse Organisatie voor Wetenschappelijk Onderzoek'').

[1] J.L. Cardy, in *Phase Transitions and Critical Phenomena*, edited by C. Domb and J.L. Lebowitz (Academic Press, London, 1987), Vol. 11, p. 55, and references therein.
[2] T.W. Burkhardt and E. Eisenriegler, J. Phys. A **18**, L83 (1985).
[3] R. Badke, V. Rittenberg, and H. Ruegg, J. Phys. A **18**, L867 (1985).
[4] T.W. Burkhardt and I. Guim, Phys. Rev. B **47**, 14 306 (1993), and references therein.
[5] J.L. Cardy, J. Phys. A **17**, L385 (1984).
[6] J.L. Cardy, Nucl. Phys. B **240**, 514 (1984); Phys. Rev. Lett. **65**, 1443 (1990).
[7] I. Reš and J.P. Straley, Phys. Rev. B **61**, 14 425 (2000).
[8] R. Rieger and N. Kawashima, Eur. Phys. J. B **9**, 233 (1999).
[9] H.W.J. Blöte and Y. Deng, Phys. Rev. E **66**, 066110 (2002).
[10] L. Onsager, Phys. Rev. **65**, 117 (1944).
[11] T.W. Burkhardt and B. Derrida, Phys. Rev. B **32**, 7273 (1985), and references therein.
[12] A. Luther and I. Peschel, Phys. Rev. B **12**, 3908 (1975).
[13] K. Binder, Phys. Rev. B **43**, 119 (1981).
[14] H.F. Trotter, Proc. Am. Math. Soc. **10**, 545 (1959).
[15] M. Suzuki, Prog. Theor. Phys. **56**, 1454 (1976).
[16] G. Kamieniarz and H.W.J. Blöte, J. Phys. A **26**, 201 (1993).
[17] Y. Deng and H.W.J. Blöte, Phys. Rev. Lett. **88**, 190602 (2002).
[18] H.W.J. Blöte and Y. Deng (unpublished).